Applied Surface Science 720 (2026) 165114

Contents lists available at ScienceDirect

Applied Surface Science

journal homepage: www.elsevier.com/locate/apsusc

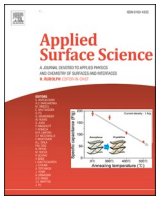

Full Length Article

In situ Al_2O_3 atomic layer deposition on pristine (0 0 1) GaAs: interface chemistry and its implication on charge carrier recombination and Fermi level pinning

Nataliya Demarina [a,*], Soraya Karimzadah [b], Benjamin Bennemann [c], Christoph Krause [c], Abdur Rehman Jalil [c], Heinrich Hartmann [d], Beata Kardynał [b], Mihail Ion Lepsa [b], Detlev Gruetzmacher [b,c]

[a] Peter Gruenberg Institute - 2, Forschungszentrum Juelich 52428 Juelich, Germany
[b] Peter Gruenberg Institute - 9, Forschungszentrum Juelich 52428 Juelich, Germany
[c] Peter Gruenberg Institute - 10, Forschungszentrum Juelich 52428 Juelich, Germany
[d] Central Institute of Engineering, Electronics, Analytics, Forschungszentrum Juelich 52428 Juelich, Germany

ARTICLE INFO

Keywords:
Pristine (001) GaAs substrate
In situ Al_2O_3 atomic layer deposition
X-ray photoelectron spectroscopy analysis
And room-temperature photoluminescence measurements

ABSTRACT

The study investigates the Al_2O_3/GaAs interface formed by *in situ* atomic layer deposition (ALD) of Al_2O_3 on pristine (0 0 1)-oriented GaAs substrate, using X-ray photoelectron spectroscopy (XPS) and room-temperature photoluminescence (PL). The Al_2O_3/GaAs interface is free of high-valence arsenic (As_2O_3 and As_2O_5) and gallium (Ga_2O_3) oxides when the Al_2O_3 layer thickness exceeds 3 nm. The Al_2O_3 deposition on an As-terminated GaAs substrate leads to the presence of low-valence arsenic oxides (As_2O and AsO) and As–As bonds related to As–As dimers at the interface. These dimers restrict the PL enhancement to approximately twice that of unpassivated GaAs. In contrast, Ga-terminated GaAs exhibits a reduction of roughly an order of magnitude in these interfacial species, as well as a PL intensity that is significantly (x20) higher than that of unpassivated GaAs. When the Al_2O_3 layer thickness is less than 3 nm, both the low- and high-valence oxides, as well as elemental As, are detected in the near-interface region of Ga- and As-terminated GaAs samples. The PL intensity of GaAs capped with an Al_2O_3 layer thinner than 3 nm is still considerably (x8) higher than that of unpassivated GaAs and is mainly limited by elemental arsenic. According to XPS data, oxide deposition reduces band bending in GaAs at the Al_2O_3/GaAs interface by 0.2–0.4 eV, indicating a decrease in interface state density, i.e. the unpinned state of the Fermi level at the interface. The study delivers criteria for the high-quality passivation of (0 0 1) GaAs surface.

1. Introduction

The use of III-V compound semiconductors has become inevitable for the future development of high frequency devices offering low noise and low thermal sensitivity as well as of optoelectronic devices for applications in solid-state electronics, wireless communication, artificial intelligence, clean energy generation and others [1]. These devices take advantage of the higher electron mobility, higher breakdown voltage, and larger direct band gap of GaAs compared to Si. However, the presence of an unstable intrinsic oxide at the high-*k*/GaAs interface results in numerous defects that would cause charge carriers to recombine before being directed to provide the required current or radiation. Additionally, in electronic devices the defects can trap charge carriers, thus degrading the channel carrier mobility. A high density of interface states fixes the Fermi level position at the interface (Fermi level pinning) preventing its modulation by the external electric field and thus degrading the gate control of the channel charge [2–5].

Typically, the high density of defects at the GaAs/oxide interface is considered to be the main reason for Fermi level pinning. The defects can be caused by the presence of atoms at the interface that do not have their normal chemical valence or are misbonded [5]. The surface of atomically clean GaAs can generally contain As and Ga dangling bonds as well as As–As and Ga-Ga bonds. The density-functional theory calculations have shown that the Ga dangling bond gives rise to a state

* Corresponding author.
E-mail address: n.demarina@fz-juelich.de (N. Demarina).

https://doi.org/10.1016/j.apsusc.2025.165114
Received 18 September 2025; Received in revised form 28 October 2025; Accepted 2 November 2025
Available online 6 November 2025

close, to the conduction band edge, the As dangling bond – to a state close to the valence band edge, and the As–As dimer – to a state just above the middle of the bandgap [5–8]. In contrast, the oxidized As or Ga itself do not appear to introduce defect levels directly in the semiconductor band gap [9]. However, GaAs oxidation is accompanied by an increase in volume. This causes strain at the interface, which can lead to oxygen-induced structural disorder and subsequent formation of the defects states in the gap. Therefore, reducing the defect density at the GaAs surface is critical for controlling the interface states that form in the semiconductor gap [10].

It is generally believed that the density of states at the GaAs surface can be reduced by surface passivation. Passivation should provide both, chemical and electronic protection of the semiconductor surface from the outside world [3]. The surface passivation material must thus be chemically stable and adhere to the semiconductor surface with sufficiently strong chemical bonds. In addition, it should have a larger bandgap than the semiconductor and terminate the dangling bonds at the semiconductor surface without forming the states in the semiconductor bandgap. Al_2O_3, as a passivation high-*k* dielectric for GaAs surface largely meets the above criteria. Moreover, Al_2O_3 layer synthesized by atomic layer deposition (ALD) conformally coats extremely complex shapes with a material layer of high quality at low temperatures (below 400 °C). ALD grown Al_2O_3 is suitable for a wide range of applications aimed at scaling down electronic devices [11]. *In situ* deposition of Al_2O_3 is considered when a dielectric oxide is deposited on the clean GaAs surface, which has not been exposed to air and thus does not contain unwanted impurities. In contrast, in the case of *ex situ* deposition, the air-exposed GaAs surface has defects introduced by oxidation and must be subjected to chemical treatment or annealing prior to Al_2O_3 deposition. However, due to the 'self-cleaning' effect of atomic layer deposited Al_2O_3, the intrinsic oxides on a GaAs surface can be removed already within the first few cycles of oxide deposition [11]. Numerous experimental [12–25] and theoretical [26,27] studies have investigated the origin of the self-cleaning effect and the Al_2O_3/GaAs interface properties after *ex situ* Al_2O_3 deposition. In general, the *ex situ* studies significantly outnumber the *in situ* studies [28–35], which is not surprising considering the difficulties in maintaining an intrinsically clean semiconductor surface prior to coating it with a high-*k* dielectric film. However, previous studies on *in situ* passivation of As-rich GaAs (0 0 1) surface exhibiting a 2×4 reconstruction, Ga-rich GaAs (0 0 1) surface having a 4×6 reconstruction and 2×2 reconstructed GaAs (1 1 1)A [31] surface showed clear advantages of the *in situ* compared to *ex situ* passivation. The capacitance–voltage (CV) measurements of metal-oxide-semiconductor capacitors of ALD-Al_2O_3 on GaAs surfaces revealed a significant decrease in a number of surface states in the semiconductor bandgap at the high-*k* dielectric/GaAs interface. Unfortunately, the measured CV characteristics still demonstrated pronounced frequency dispersion in the accumulation regime [29,32–35]. This fact led to the conclusion that the *in situ* approach used for ALD Al_2O_3 may not be sufficient to passivate the GaAs surface [28,29,32,35].

In our study, we revisit the *in situ* approach for passivation of (0 0 1) oriented GaAs surface with ALD Al_2O_3. This allows us to take advantage of the contamination-free GaAs surface at the beginning of the deposition process. However, we go beyond the scope of previous studies and investigate the *in situ* Al_2O_3 ALD process in detail, namely varying the sequence and number of precursor pulses at the deposition beginning, the deposition temperature and the thickness of the deposited Al_2O_3 layer. We use *ex situ* X-ray photoelectron spectroscopy analysis to characterize the surface reactions associated with the *in situ* atomic layer deposition of Al_2O_3 on GaAs. The optical method, based on the room temperature photoluminescence measurements of the passivated GaAs samples is used to get insight into the impact of defects at the Al_2O_3/GaAs interface on the radiative recombination of electron-hole pairs.

2. Experimental section

2.1. Fabrication of the GaAs samples in situ passivated with Al_2O_3

The GaAs samples are fabricated in a multi-chamber growth system consisting of a Scienta Omicron molecular beam epitaxy (MBE) chamber and a FlexAL®II ALD reactor developed by Oxford Instrument Plasma Technology, connected by transfer modules maintaining ultra-high vacuum of 10^{-9} Torr. MBE is employed to grow a GaAs layer on a GaAs (1 0 0) wafer at a temperature of 610 °C. The grown layers are unintentionally *p*-doped with a doping level below 10^{14} cm^{-3}. The freshly grown GaAs samples have As-rich atomically ordered surface with (2 × 4) reconstruction (α-phase), which is verified by reflection high-energy electron diffraction (RHEED) in the MBE growth chamber. This type of the reconstruction is stable and most commonly obtained during MBE growth at substrate temperatures above 550 °C [36]. To maintain the As-terminated surface in the (2 × 4) reconstruction, we cool down the epitaxially grown GaAs sample with the As_4 flux still on. The Ga-rich (1 × 1) surface is prepared after the MBE growth of the GaAs layer by cooling the sample down to 400 °C with As_4 decreasing flux in the MBE chamber and then unloading the wafer. Prior to Al_2O_3 deposition, the Ga-terminated samples are additionally annealed at 500 °C for 10 min in the preparation chamber (the vacuum level of low 10^{-9} Torr). Fig. S1 of the Supplementary Information (SI) shows RHEED patterns of the MBE grown As- and Ga-terminated surfaces of a GaAs substrate before its transfer to the ALD chamber.

Within the *in situ* passivation approach, Al_2O_3 is deposited on the clean and atomically ordered surface of the selected GaAs samples in the ALD reactor at the substrate temperature of 250 and 300 °C. The trimethylaluminum ($Al(CH_3)_3$, TMA) is used as the metal–organic precursor and the oxygen source in the oxide is deionized water (H_2O). Ar is employed as the carrier and purge gas. Table 1 summarizes the samples prepared for this study.

2.2. Characterisation methods

The analysis of the Al_2O_3/GaAs interface is performed *ex situ* by monochromatic *X*-ray photoelectron spectroscopy using an Al *K* α (1486.6 eV) X-ray source. High resolution spectra are taken for several core levels, namely arsenic (As 3*d* and As $2p_{3/2}$), gallium (Ga 3*d* and Ga $2p_{3/2}$), aluminum (Al 2*p*) and oxygen (O 1*s*) using a step size of 0.1 eV

Table 1
Studied samples.

Name	GaAs surface termination	Additional step prior to the deposition	Al_2O_3 thickness (nm) (XRR)	O/Al ratio
As-10-st	As	–	10.4 ± 0.1	1.5 ± 0.1
As-10-4TMA	As	4 TMA pulses	10.3 ± 0.1	1.7 ± 0.2
As-10-5H_2O	As	5 H_2O pulses	10.3 ± 0.1	1.5 ± 0.1
As-10-st-250	As	–	9.9 ± 0.1	1.4 ± 0.1
As-5-st	As	–	5.9 ± 0.1	1.8 ± 0.2
As-2-st	As	–	2.8 ± 0.1	–
As-2-5H_2O	As	5 H_2O pulses	2.8 ± 0.1	1.5 ± 0.1
Ga-12-5H_2O	Ga	5 H_2O pulses	12.2 ± 0.1	1.4 ± 0.1
Ga-12-st	Ga	–	12.2 ± 0.1	1.4 ± 0.1
Ga-12-4TMA	Ga	4 TMA pulses	11.6 ± 0.1	1.4 ± 0.1
Ga-3-5H_2O	Ga	5 H_2O pulses	3.2 ± 0.1	1.7 ± 0.2
Ga-2-5H_2O	Ga	5 H_2O pulses	2.2 ± 0.1	1.7 ± 0.2

and a bandpass energy of 23.5 eV. The spectra are collected at a photoelectron emission angle of 45° with respect to the sample surface. Charge correction is performed by setting the GaAs component of the As $3d_{5/2}$ peak to 40.7 eV. The samples with Al_2O_3 layer thicker than 3 nm require thinning of the oxide layer below the typical XPS probe depth (about 3–9 nm) determined by the inelastic mean free path of photoelectrons [37]. The Al_2O_3 layer of these samples is partially etched with the Ar^+ ions inside the XPS tool prior to XPS data collection. The details of the etching are discussed in Section 2 of SI. The deconvolution of the XPS spectra is performed using Shirley-type background subtraction and Voigt functions for peak fitting. Similar to the study by Hinkle *et al.* on the detection of different Ga and As components in the XPS spectra of GaAs [12–16], we fit the measured XPS spectra with the minimum number of the peaks and additional peaks are added only when the correct fit is not feasible without their inclusion.

The thickness of the deposited Al_2O_3 layer is controlled by X-ray reflectivity measurements (XRR). PL measurements of the GaAs samples are performed with an inVia Raman microscope in PL mode at room temperature (300 K) using 532 nm excitation with a laser power of 0.05 and 0.1 % from the maximum (0.08 and 0.14 mW, correspondingly).

3. Results

3.1. Native oxides composition on the GaAs surface subject to ambient air at room temperature

At the beginning of our study, we briefly focus on the oxides composition formed on the freshly MBE grown GaAs layer exposed to ambient air. In this experiment, XPS measurements are performed on the sample after 1 day and 6 months of exposure to air at room temperature. This investigation allows us to reveal the difference between the chemical compositions of native oxides/GaAs and Al_2O_3/GaAs interfaces.

We study the distribution of different chemical bonds, i.e. compounds near the surface, by comparing 2*p* and 3*d* photoelectron spectra. The analysis is based on the fact that the core-level electrons of the As 3*d* and Ga 3*d* photoelectron spectra have low binding energies (about 40 and 20 eV, respectively), hence, high kinetic energies (1446 and 1468 eV, respectively). The photoelectrons with the high kinetic energy have the inelastic mean free path about $\lambda_e = 3.1$ nm [37] and can escape from relatively deep in the GaAs semiconductor, i.e. allowing us to get insight into the bulk of the GaAs layer. The 3*d* electrons represent a weighted average of the entire surface layer and also the GaAs bulk. In contrast, As 2*p* and Ga 2*p* photoelectrons (the binding energy (BE) of 1323 and 1117 eV, respectively) have a kinetic energy of about 164 and 370 eV, resulting in inelastic mean free paths of $\lambda_e = 0.7$ and 1.1 nm, respectively. Therefore, the information provided by the 2*p* photoelectrons refers roughly to the top few atomic layers of the GaAs surface layer.

We analyze the native oxides on the GaAs surface by first focusing on the As 3*d* and Ga 3*d* and then on the more surface sensitive As $2p_{3/2}$ and Ga $2p_{3/2}$ photoelectron spectra [38]. After subtraction of the background signal, the As 3*d* and Ga 3*d* photoelectron spectra of the native oxide covered GaAs sample are shown in Fig. 1 (a). Deconvolution of the As 3*d* spectrum allows the resolution of two spin–orbit split doublets. The intensity ratio for the Ga 3*d* and As 3*d* doublets is fixed at 3:2 and the spin–orbit splitting is at 0.44 and 0.7 eV, respectively. The strongest doublet is related to As in the GaAs bulk with peaks corresponding to the As $3d_{5/2}$ (40.7 eV) and As $3d_{3/2}$ (41.4 eV) states (fitted blue lines). This doublet is accompanied by a weak doublet (41.2 and 41.9 eV) positively shifted in energy by ΔBE=+0.5 eV with respect to the GaAs bulk signal (fitted green lines). In accordance with previous studies [31,39], the doublet originates from As–As bonding from As_{Ga} antisites or As interstitials [40]. Fitted peaks at 44.0 and 45.2 eV (shifted by ΔBE=+3.3 and +4.5 eV with respect to the As–Ga peak) are assigned to the As–O bond in As_2O_3 and As_2O_5 oxides, correspondingly. The Ga 3*d* spectrum was fitted with two peaks (at 18.9 and 19.3 eV) representing the contribution of Ga $3d_{5/2}$ and Ga $3d_{3/2}$ in the bulk GaAs. The peak shifted by ΔBE = +1.2 eV from the bulk (at 20.3 eV) is caused by photoemission from Ga-O bonds in the Ga_2O_3.

Fig. 1(b) displays the As $2p_{3/2}$ and Ga $2p_{3/2}$ photoelectron spectra of this sample. The As 2*p* spectrum shows five peaks attributed to the As–Ga bond (in bulk GaAs at 1322.6 eV), the As–As bond (elemental As

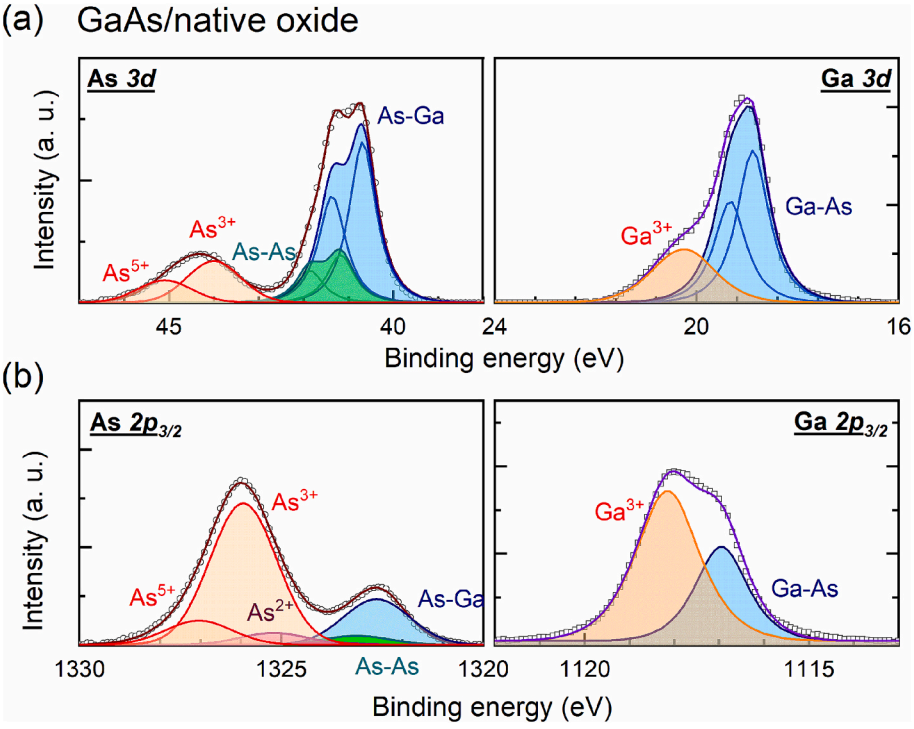

Fig. 1. Photoelectron spectra for (a): the As 3*d* (left) and Ga 3*d* (right) and (b): the As 2*p* (left) and Ga 2*p* (right) core-level features after MBE-grown GaAs layer has been 1 day exposed to ambient air at room temperature.

and shifted with ΔBE = +0.5 eV with respect to the bulk As–Ga peak) and the arsenic oxidation states As^{2+} (ΔBE = +2.55 eV, AsO), As^{3+} (ΔBE = +3.3 eV, As_2O_3), and As^{5+} (ΔBE = +4.4 eV, As_2O_5) [41]. The Ga $2p_{3/2}$ plot shows chemical states attributed to the Ga–As bond (in bulk GaAs at 1116.9 eV) and Ga–O bond (in Ga_2O_3 at 1118.1 eV and ΔBE = +1.2 eV with respect to the bulk Ga–As peak).

Analysis of the 2*p* and 3*d* data (SI, Section 4) shows that a mixture of the Ga and As oxides is mostly present in the upper part of the GaAs layer with Ga_2O_3 as the dominant oxide. The relative fraction of As atoms forming As–As bonds calculated from the 2*p* spectrum (Fig. S3 (a, b), SI) is much lower than that from the 3*d* spectra. This indicates that the As atoms are mostly present at the interface between GaAs and the native GaAs oxides. The formation of elemental As can be seen as a consequence of the much stronger affinity of Ga than As for binding to oxygen [42], leading to predominant Ga_2O_3 formation and As enrichment near the oxide-GaAs interface [42,43] (e.g. $As_2O_3 + 2\,GaAs \rightarrow Ga_2O_3 + 4As$). The elemental arsenic remains in the deepest oxide layer where it cannot diffuse away or oxidize again due to the low oxygen diffusivity through the finally formed oxide layer. Note, that an excess of unoxidized As atoms can diffuse into GaAs to form As interstitials or As_{Ga} antisites, causing the formation of the states deep in the bandgap [8].

3.2. *In situ passivation of GaAs surface with 10 nm thick layer of Al_2O_3*

3.2.1. *Analysis of Al_2O_3/GaAs interface formed after in situ deposition of 10 nm Al_2O_3 on the as-terminated GaAs surface*

First, we focus on the passivation of the freshly grown As-terminated polar (0 0 1) GaAs surface, a surface which has the α-phase (2 × 4) reconstruction (Fig. S1 (a), SI). The atomic structure of the α-phase can be described by the so called β2 (2 × 4) model with the ideal unit cell containing two As–As dimers in the outermost atomic layer and one As–As dimer in the third atomic layer below the surface, located within a trench formed by missing dimers in the outermost layer [36,44].

The 10 nm thick Al_2O_3 layer was deposited *in situ* at 300° C (sample As-10-st in the Table 1). In addition to protecting the GaAs surface from further formation of the native oxides, we aim to decompose the As–As dimers present at the surface and causing states in the bandgap. Following Ref. [8], we begin the deposition of Al_2O_3 on the As-terminated GaAs surface with a TMA pulse, expecting that the small TMA molecules will insert into the As–As bonds and break them. We perform the 'standard' deposition of Al_2O_3 with a cycle consisting of TMA pulse, purge pulse of high purity Ar, pulse of deionized water, purge pulse of Ar. The deposition of 10 nm thick Al_2O_3 film takes about 100 cycles.

Fig. 2 (a) shows the cross-sectional TEM image of the Al_2O_3/GaAs specimen, indicating the formation of a uniform continuous amorphous Al_2O_3 film. However, the presence of some interface region between the Al_2O_3 and GaAs layers is observed in Fig. 2 (b).

The chemical properties of Al_2O_3/GaAs structures are studied by XPS. The inset of Fig. 3 (a) shows the Al 2*p* spectrum with only one peak assigned to the Al-O bond in Al_2O_3 and this, together with the TEM micrograph (Fig. 2), confirms the successful growth of Al_2O_3 on the GaAs surface. The O/Al ratio calculated from the measured Al 2*p* and O 1*s* spectra for all investigated samples is in the range of 1.4 ± 0.1 to 1.7 ± 0.2 (Table 1), which is close to the ideal value of 1.5, indicating a high stoichiometry of the grown oxide. The spectra of As 3*d* core-levels of GaAs substrate with *in situ* deposited Al_2O_3 layer (Fig. 3(a)) can be decomposed into only two doublet components. Besides the main component caused by photoelectrons with participation of bulk crystal As–Ga bonds (at 40.7 and 41.4 eV), an additional component can be distinguished at 41.1 and 41.8 eV (ΔBE = +0.4 eV). We attribute this feature to the contribution of As–As bonds. The spectrum of Ga 3*d* core levels is fitted with a doublet component (at 18.9 and 19.3 eV) and is assigned to the Ga–As bond of bulk GaAs.

Fig. 3(b) displays the As $2p_{3/2}$ and Ga $2p_{3/2}$ core-level spectra of the As-terminated GaAs films with *in situ* deposited 10 nm Al_2O_3. The Ga

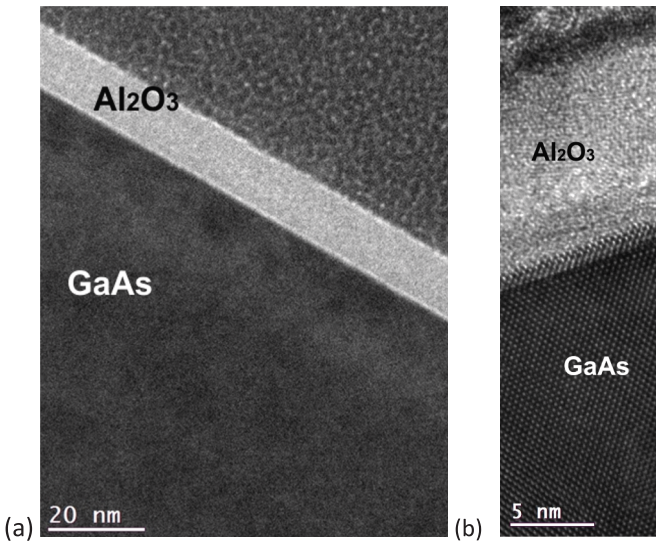

Fig. 2. TEM micrograph of the Al_2O_3 layer *in situ* deposited at 300 °C on the MBE grown GaAs layer: (a) Overview image of the Al_2O_3/GaAs structure; (b) Crystal structure at the Al_2O_3/GaAs interface.

$2p_{3/2}$ spectra (Fig. 3(b)) consists of only one peak at 1116.9 eV, which we attribute to the Ga–As bond. The As core signal requires three components for a proper fit. One of them corresponds to the As–Ga bond in bulk GaAs (at 1322.4 eV). This component is red-shifted by about 0.2 eV with respect to the similar As–Ga bond peak in the native oxides/GaAs sample. The As–As component, present in the As $2p_{3/2}$ spectrum of the GaAs with native oxides (Fig. 1(b)) has been replaced by the new As^- component. It is red-shifted by about 0.4 eV from the As–Ga peak (ΔBE = −0.4 eV) and is often attributed to As–As dimers or dangling bonds at the GaAs surface [45–47]. The two other peaks, i.e. As^{1+}, As^{2+}, we assign to the oxidation states As^{1+} (ΔBE = +1.3 eV) and As^{2+} in the oxides As_2O and AsO, respectively.

The origin of these As–As dimers and oxidation states is discussed in the detailed *in situ* XPS analysis of the Ga/As core-level 3*d* spectra measured during the deposition of Al_2O_3 on the atomically clean As-rich GaAs (0 0 1)-2 × 4 surface [28,31]. The study shows that the GaAs surface reacts with TMA through the surface As. After one cycle of TMA and water, only the As–As dimers of the first surface layer are affected by the precursors in such a way that they can bond to oxygen, which in turn bonds to Al in $Al(CH_3)_2$. Thus, the As–O–Al -$(CH_3)_2$ configuration is formed. The same study states that after already 10 ALD cycles, some of the As–O–Al bonds break into As–O bonds, implying the formation of an arsenic oxide with As atoms in the 1+/2 + charge state at the GaAs/Al_2O_3 interface. Some of the As–O–Al bonds that have not been transformed into As–O bonds may evolve into As–Al bonds some time after Al_2O_3 deposition [31]. The latter is also confirmed by our measurements of Al 2*p* spectra performed 6 months after Al_2O_3 deposition (Fig. 3, a (inset)). In addition to the Al–O bond, there is a distinct peak that we attribute to the Al-As bond. The same study shows that the As–As dimers located in the third surface layer are not affected by the TMA and water pulses, and could be the origin of the As^--component in the As $2p_{3/2}$ spectrum.

We should note that first-principle calculations have shown that the existence of the As–O–Al bond as well as low-valence As oxides at the Al_2O_3/GaAs interface is not accompanied by the formation of additional states in the GaAs bandgap [9,48].

The As 3*d*, Ga 3*d*, As 2*p* and Ga 2*p* spectra measured on the same sample after 6 months (Fig. S5 in SI) do not show the appearance of the high valence oxides at the GaAs/Al_2O_3 interface. However, the As–As dimers and $As^{1+/2+}$ oxidation states are still present at the interface and their amount has hardly changed. The latter is a clear indication that the

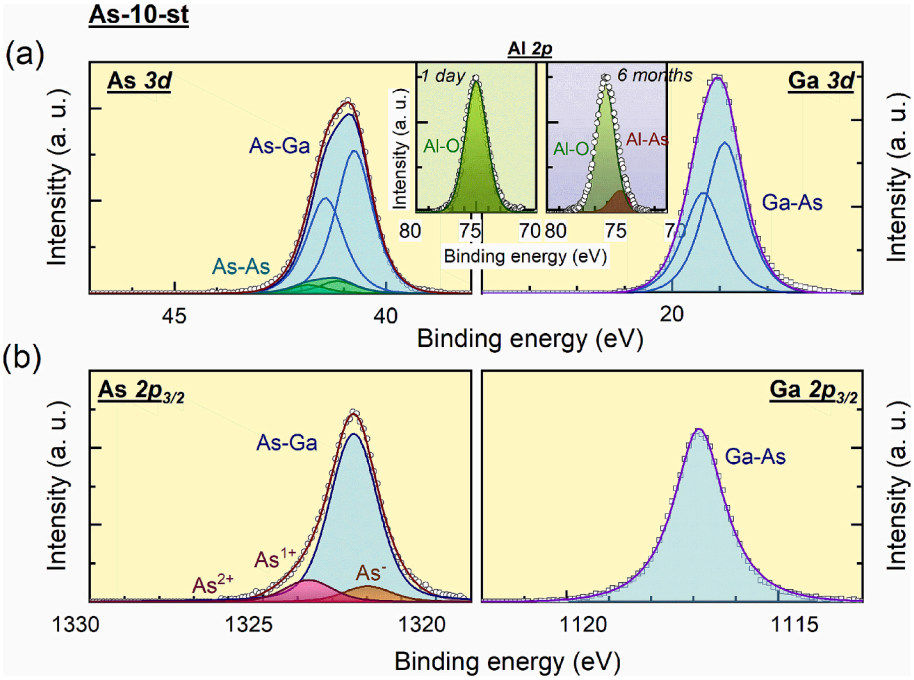

Fig. 3. Photoelectron spectra (sample As-10-st) for (a): the As 3*d* (left) and Ga 3*d* (right) and (b): the As $2p_{3/2}$ (left) and Ga $2p_{3/2}$ (right) core-level features. Inset: Photoelectron spectra for the Al 2*p* measured 1 day (left) and 6 months (right) after the deposition of 10 nm of Al_2O_3.

in situ deposited Al_2O_3 layer of 10 nm thickness reliably protects the GaAs surface from post-deposition oxidation.

It is intuitively clear that the first ALD cycle may be central in determining the properties of the GaAs/Al_2O_3 interface. To reduce the amount of As–As dimers and As^{1+} and As^{2+} oxidation states, we vary the sequence of precursor pulses at the beginning of the standard Al_2O_3 deposition. Namely, we perform additional experiments and expose the surface of the freshly grown GaAs to 4 TMA pulses (sample As-10-4TMA) or 5 H_2O pulses (sample As-10-5H_2O). A purge pulse of Ar follows every single additional TMA or H_2O pulse. The initial pulses are followed by complete TMA/H_2O cycles of 'standard' deposition. The deposition temperature remains at 300 °C and the targeted thickness of the deposited Al_2O_3 layer is about 10 nm. We expect that increasing the number of TMA pulses prior to the standard deposition procedure will improve the coverage of the GaAs surface with TMA molecules and thus intensify the corresponding chemical reactions. On the other hand, replacing one TMA pulse with a water pulse at the beginning of the deposition might change the character of the chemical bonds at the interface. In both cases, the measured XPS spectra (Fig. S6 and S7, SI) are qualitatively similar to those presented in Fig. 3(a) and (b), indicating that the GaAs/Al_2O_3 interface was free of the As_2O_3, As_2O_5 and Ga_2O_3 species. The As–As dimers and $As^{+1/+2}$ oxidation states remain present at the GaAs/Al_2O_3 interface. However, their amount varies slightly depending on whether the deposition starts with a TMA or a water pulse (Fig. S9, SI).

We have performed an additional experiment by reducing the Al_2O_3 deposition temperature to 250 °C. Both 3*d* and 2*p* XPS spectra (Fig. S8, SI) show peaks, which are completely identical to those presented in Fig. 3 (a) and (b) with only slightly changed contribution of the As–As dimers and As^{1+}/As^{2+} oxidation states (Fig. S9, SI).

3.2.2. *Analysis of the Al_2O_3/GaAs interface formed after in situ deposition of 10 nm Al_2O_3 on the Ga-terminated GaAs surface*

The evidence that the *in situ* deposition of Al_2O_3 on the As-terminated GaAs surface buries some of the As–As surface dimers and also leads to the formation of the low-valence As oxides at the oxide/GaAs interface suggests that the use of the Ga- instead of the As-terminated surface might be a possible way to obtain the desired defect-free interface. Furthermore, previous experiments [49,50] have shown that the *in situ* molecular beam deposition of Al_2O_3 on the Ga-rich reconstructed GaAs surfaces results in a significant reduction of the surface state density and improves the device performance. Following the suggestion of Refs. [8,48] that according to the electron counting rule [51] the Ga termination on the GaAs side should be matched by the O termination of Al_2O_3, we start the oxide deposition with 5 water pulses followed by the 'standard' procedure of TMA and water pulses. Deposition is performed at 300 °C. According to Ref. [52], H_2O preferentially interacts with Ga atoms, and only a small effect is observed on the minor surface As atoms, which act as "neighbors" and may eventually assist in water dissociation into OH and H at the GaAs surface. The OH dissociation product interacts with Ga atoms to form hydroxide species, while the H interacts with an As atom. When the first TMA pulse arrives at an OH– or H-terminated surface, its methyl ligands can react with surface hydrogen, releasing CH_4 and leading to the formation of Ga–O–Al and As–Al bonds. The subsequent water pulse then removes the remaining methyl groups, again releasing CH_4, as the "ligand exchange" is the main growth mechanism.

The Al 2*p* spectrum shown in Fig. 4, inset, indicates successful growth of the Al_2O_3 layer with an O/Al ratio of 1.4 ± 0.1 (Table 1). The spectra of As 3*d* core-levels (Fig. 4(a)) can be decomposed this time into two doublet components. Along with the main component caused by the photoelectrons participating in As–Ga bonds of a bulk crystal (at 40.7 and 41.4 eV), an additional component can be distinguished at 41.3 and 42.0 eV (ΔBE = +0.5 eV), which is assigned to the contribution of As–As bonds. The spectrum of the Ga 3*d* core levels is fitted with a doublet component (at 18.8 and 19.3 eV) and is assigned to the Ga–As bond of bulk GaAs. Fig. 4(b) displays the As $2p_{3/2}$ and Ga $2p_{3/2}$ core-level spectra of the Ga-terminated GaAs. Both As $2p_{3/2}$ and Ga $2p_{3/2}$ photoelectron signals consist of only one dominant peak at 1322.3 eV and 1116.7 eV, respectively, which we attribute to the As–Ga (Ga–As) bond. The As $2p_{3/2}$ spectrum also contains a weak peak at 1323.6 eV, which we assign to the As_2O oxide. In contrast to the As-terminated GaAs substrate, the intensity of the peak corresponding to As–As dimers is reduced by an order of magnitude and is not seen in the As $2p_{3/2}$ spectrum. Considering

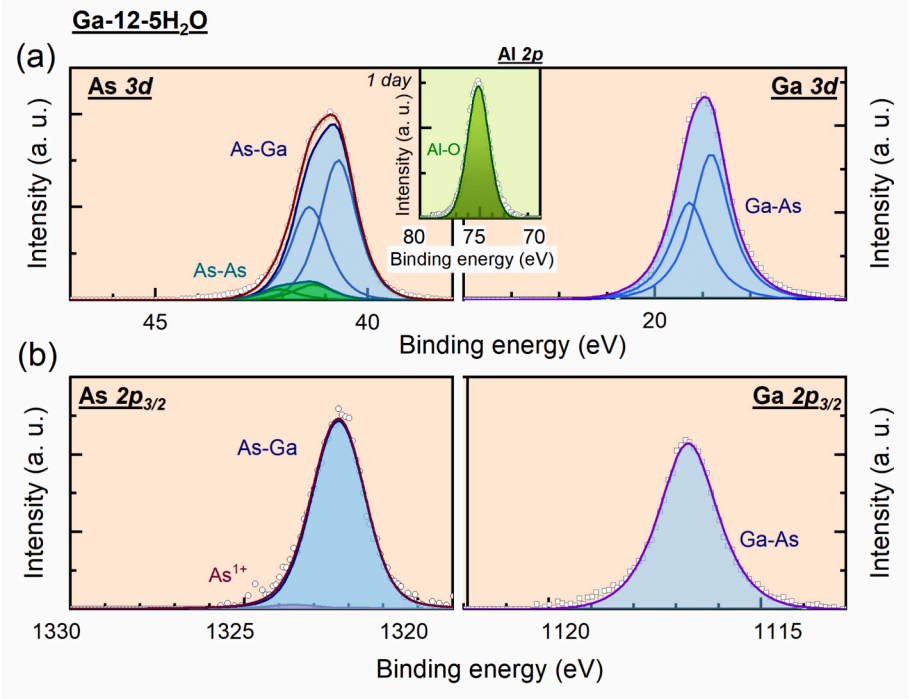

Fig. 4. Photoelectron spectra (sample Ga-12-5H_2O) for (a): the As 3*d* (left) and Ga 3*d* (right) and (b): the As $2p_{3/2}$ (left) and Ga $2p_{3/2}$ (right) core-level features. Inset: Photoelectron spectra for the Al 2*p* measured 1 day after Al_2O_3 deposition.

the idea that the onset of oxide growth might affect the interface quality, we perform two additional experiments using the 'standard' Al_2O_3 deposition procedure (sample Ga-12-st) and exposing the surface of the freshly grown GaAs to 4 TMA pulses before the 'standard' deposition (sample Ga-12-4TMA). In addition to the Ga–As species corresponding to bulk GaAs, the measured As 3*d*, Ga 3*d*, As $2p_{3/2}$ and Ga $2p_{3/2}$ spectra show the presence of only low amount of As^{1+} oxidation states and very tiny fraction of As–As dimers at the interface (Fig. S9-S11, SI).

3.3. *In situ passivation of GaAs surface with thinner (below 10 nm) layer of Al_2O_3: Oxide re-growth at the Al_2O_3/GaAs interface*

For high efficiency operation of modern nanometer devices, the desirable thickness of the deposited high-*k* dielectric should be reduced. Therefore, as a next step, we perform *in situ* deposition of Al_2O_3 with a thickness below 10 nm on the As- and Ga-terminated GaAs substrate. The deposition temperature is 300 °C. For the As-terminated surface we follow the 'standard' deposition procedure. The Al_2O_3 growth on the Ga-terminated surface begins with 5 H_2O pulses. The thickness of the grown

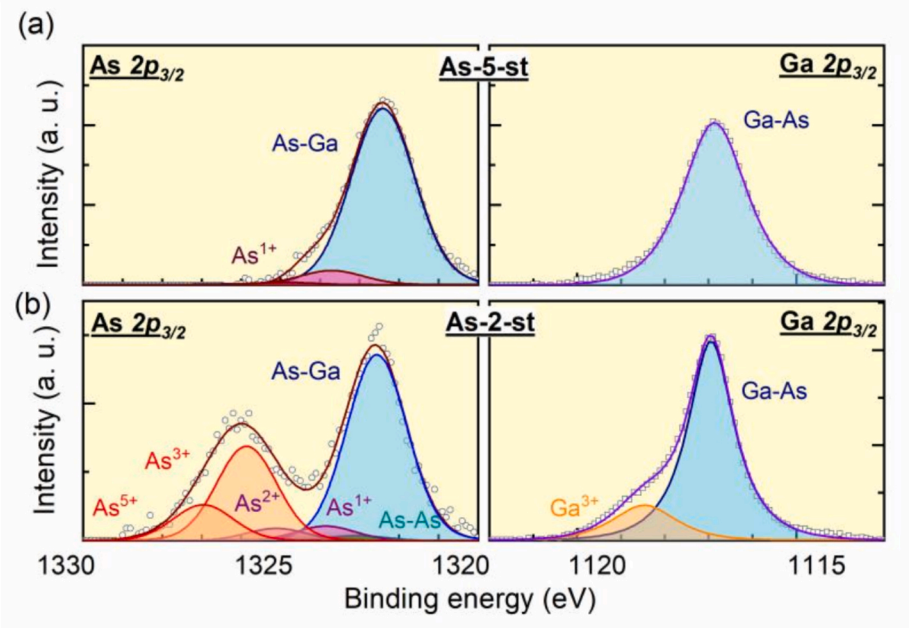

Fig. 5. Photoelectron spectra for the As $2p_{3/2}$ (left) and Ga $2p_{3/2}$ (right) core-level features after *in situ* deposition of 5.8 nm (a) and 2.8 nm (b) Al_2O_3 on the As-terminated GaAs substrate.

Al_2O_3 layer is 5.9 and 2.8 nm for the As-terminated and 3.2 and 2.2 nm for the Ga-terminated GaAs samples.

In Figs. 5 and 6 we compare the As $2p_{3/2}$ and Ga $2p_{3/2}$ core-level spectra obtained for the As- and Ga-terminated GaAs samples with Al_2O_3 of different thickness. It can be seen that the Al_2O_3/GaAs interface formed after the deposition of 3 or 5 nm thick Al_2O_3 layer possesses As^{1+} oxidation state. This is similar to the main feature of the samples passivated with Al_2O_3 thicker than 10 nm (Figs. 3 and 4). However, the persistent As–As dimer peak (As^-) typical of the As-terminated GaAs samples (Fig. 3 and S5-S8 of the SI) is no longer detected.

In contrast, after 2 nm Al_2O_3 deposition, the As $2p_{3/2}$ and Ga $2p_{3/2}$ spectra resemble those measured for GaAs with native oxides (Fig. 1). Namely, the Ga–As (As–Ga) feature corresponding to bulk GaAs is greatly reduced, while the Ga and As oxide peaks become strongly pronounced. The As–O feature in the both cases, i.e. As- and Ga-terminated GaAs (Figs. 5 and 6), has four oxidation states, As^{1+}, As^{2+}, As^{3+}, As^{5+}, corresponding to As_2O, AsO, As_2O_3 and As_2O_5. The Ga-O feature includes one oxidation state, Ga^{3+}, assigned to Ga_2O_3. We attribute the presence of Ga and As oxides to interfacial oxide regrowth after the GaAs samples with thin (below 3 nm) Al_2O_3 oxide layer were exposed to ambient air [41]. The oxidation of the interface occurs due to oxygen diffusion through the thin amorphous Al_2O_3 film [53,54]. XPS measurements performed on the same samples six months later showed that the post-oxidation process continues in time and the amount of the gallium and arsenic oxides gradually increases. Next, it is important to note that persistent As–As dimers are not detected at the interface. However, in the As $2p_{3/2}$ spectrum, a new feature (As-As), blue shifted by 0.5 eV with respect to the As–Ga peak, is detected for both initially Ga- and As-terminated GaAs samples. We assign this peak to the As–As bonds of elemental As, which could be formed by the transformation of the surface As oxide reacting with the GaAs substrate (Section 3.1). It is important to note that the Ga- and As-terminated samples that have undergone the post-oxidation now show qualitatively similar interface sensitive As $2p_{3/2}$ spectra, i.e. both do not show the presence of As–As dimers. We suggest that this is due to the diffusion of oxygen through the Al_2O_3 layer. Oxygen interacts with remaining As–As dimers on the As-terminated surface, decomposing them and reducing their concentration below the detection limit.

The As *3d* and Ga *3d* spectra (Figs. S12 and S13, SI) illustrate that the amount of As^{2+} (AsO), As^{3+} (As_2O_3), As^{5+} (As_2O_5), Ga^{3+} (Ga_2O_3) oxidation states is below the detection limit of the XPS measurements for the samples with the Al_2O_3 thickness around 2.8 nm. While strongly reduced, the As^{3+} and Ga^{3+} oxidation states are detected in the near surface region when the Al_2O_3 thickness is further reduced to 2.2 nm (Fig. S13 (b), SI). This is due to the post-oxidation processes mediated by oxygen diffusion through the thinner Al_2O_3 layer. In conclusion, a reliable protection of the GaAs surface from oxidation in ambient air requires that the thickness of the *in situ* deposited Al_2O_3 layer exceeds 3 nm. This is in agreement with previous studies [21,22,41].

3.4. Reduced bend bending at the Al_2O_3/GaAs interface formed via in situ Al_2O_3-ALD on GaAs

The important question remains whether the *in situ* deposition of the Al_2O_3 layer reduces the amount of defect states at the GaAs surface, thus freeing the Fermi level at the interface. To answer this question, we compare the binding energy of the As $2p_{3/2}$ and Ga $3p_{3/2}$ core levels without and after Al_2O_3 deposition. The diagram showing the conduction and valence bands as well as the core levels is presented in Fig. 7 (a) for the GaAs sample without and with the Al_2O_3 passivation layer. The Fermi level is pinned at the surface covered with the native oxides about 0.5 and 0.7 eV above the valence band edge in the case of *p*- and *n*-type doping of the GaAs [55–57]. We assume a non-intentional *p*-doping of GaAs with a doping concentration of about 10^{14} cm^{-3}, so we can expect that according to Ref. [58], the pinning position occurs near the center of the band gap, i.e. 0.6 eV above the valence band minimum. On the other hand, at room temperature, the Fermi level is located about 0.2 eV above the valence band edge in bulk GaAs far from the GaAs surface. Thus, the band bending (E_{bb}) at the surface of the air-oxidized GaAs sample is approximately 0.4 eV. The bands and core levels are bent downward (Fig. 7, a). The strength of the bending can be characterized by the binding energy of the As $2p_{3/2}$ (Ga $2p_{3/2}$) signal, which is determined by the electrons originating from the GaAs/air (Fig. 7, a (left)) or GaAs/Al_2O_3 (Fig. 7, a (right)) interface. The stronger band bending corresponds to the higher value of $E_{b\ As\ 2p3/2}$ ($E_{b\ Ga\ 2p3/2}$). The relations $\Delta E_1=(E_{b\ As\ 2p3/2})_{air/GaAs}$- $(E_{b\ As\ 2p3/2})_{Al2O3/GaAs}$ and $\Delta E_2=(E_{b\ Ga\ 2p3/2})_{air/GaAs}$- $(E_{b\ Ga\ 2p3/2})_{Al2O3/GaAs}$ describe the difference of the band bending at the native oxides/GaAs and Al_2O_3/GaAs interfaces. The negative value

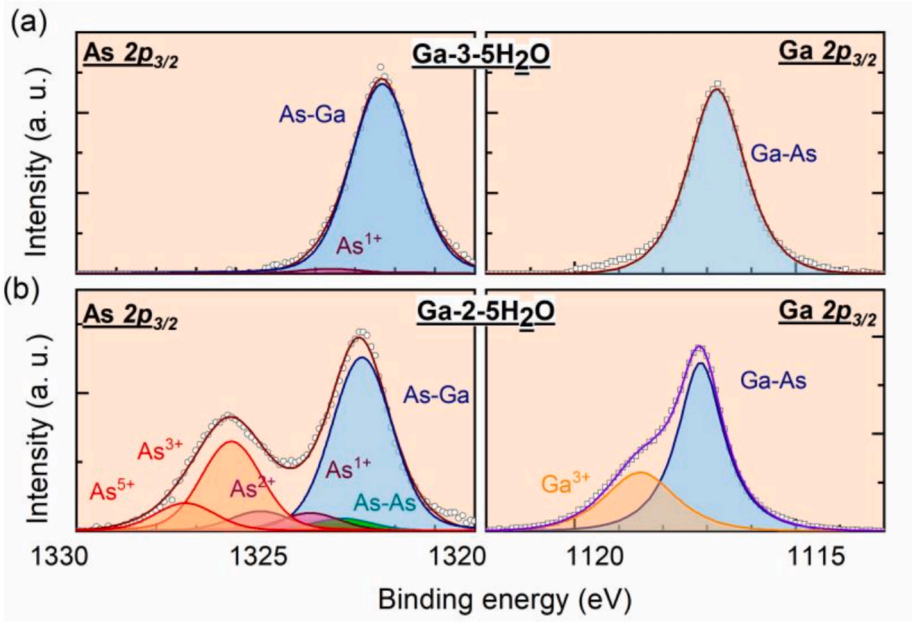

Fig. 6. Photoelectron spectra for the As $2p_{3/2}$ (left) and Ga $2p_{3/2}$ (right) core-level features after *in situ* deposition of 3.2 nm (a) and 2.2 nm (b) Al_2O_3 on the Ga-terminated GaAs substrate.

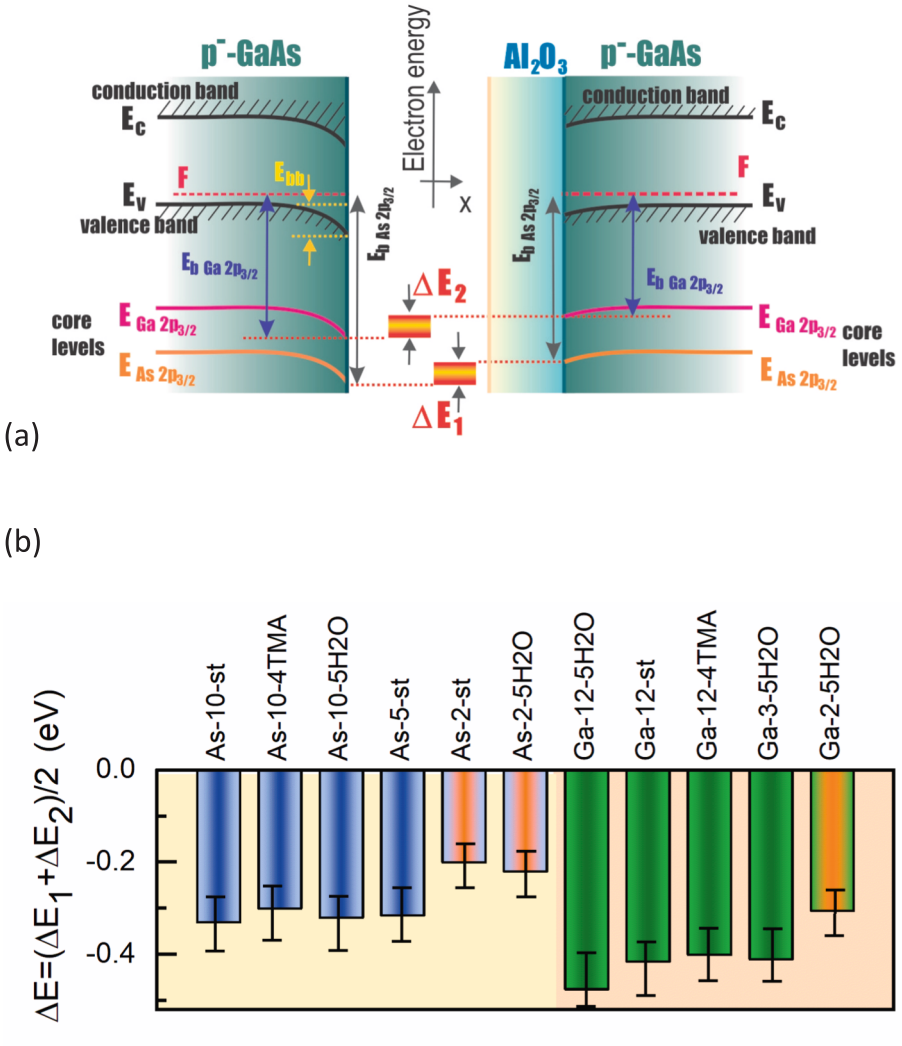

Fig. 7. (a): Schematic energy-band diagram for an abrupt p^--GaAs/air (left) and p^--GaAs/Al_2O_3 interface; shown are the valence (E_v) and conduction (E_c) band edges, the Fermi level (F) at the interface, As $2p_{3/2}$ and Ga $2p_{3/2}$ ($E_{As\ 2p3/2}$ and $E_{Ga\ 2p3/2}$) core levels and the corresponding binding energy ($E_{b\ As\ 2p3/2}$ and $E_{b\ Ga\ 2p3/2}$), the GaAs band bending (E_{bb}). (b) Averaged reduction of the band bending ($(\Delta E_1+\Delta E_2)/2$) at the GaAs surface after *in situ* deposition of Al_2O_3.

of ΔE (Fig. 7, b), which we calculate as the average between the two values ΔE_1 and ΔE_2, indicates that the band bending in the sample with the top Al_2O_3 layer deposited decreases by (0.2–0.3) ± 0.1 eV after Al_2O_3 deposition on the As-terminated surface and by (0.25–0.45) ± 0.1 eV for the Ga-terminated surface. This obviously implies that the Fermi level at the Ga-rich GaAs/Al_2O_3 interface has become unpinned and the GaAs/Al_2O_3 system has entered the flat band regime. The reduced band bending at the Al_2O_3/GaAs interface is also an indirect sign of a lower density of interface states. Finally, we would like to point out that the error in the position of the Fermi level is related to the 0.1 eV step that was used when recording the As $2p_{3/2}$ and Ga $2p_{3/2}$ photoelectron spectra.

3.5. *Optical characterization of the states at in situ-ALD Al_2O_3/GaAs interface*

We get insight into the surface recombination of the GaAs/Al_2O_3 interface using the PL spectroscopy [59,60]. The principle of the method is shown schematically in Fig. 8 (inset). Photocarriers generated by illumination of the semiconductor recombine radiatively but also via various non-radiative recombination channels. The latter reduces the intensity of the photoluminescence. Surface recombination is the largest source of excitation loss in high quality, undoped GaAs. It is dependent on surface preparation, as it may change density of the interface states at the GaAs/Al_2O_3 interface. The increase in band-to band PL intensity due to surface passivation would be a clear indication of the decreased density of states at the oxide/GaAs interface.

The laser with a wavelength of 532 nm is used for the excitation of the GaAs substrate with the deposited Al_2O_3 layer. Since we only collect a fraction of PL that enters the objective lens, we compare the intensities of the PL with the intensity of the PL of the GaAs sample with the native oxides. The PL intensity, measured at different places on the sample surface varies by no more than 20 % from its average value. We also observe a decay of the PL intensity after irradiation of the samples with the excitation power above 0.1 mW [61]. To avoid this effect, PL spectra are measured at a low excitation power of 0.05 mW. Fig. 8(a, b) shows the PL intensity obtained from the GaAs/Al_2O_3 and native oxides/GaAs samples. The spectra exhibit a maximum at 1.42 eV, which is related to band-to-band recombination in GaAs at room temperature. Fig. 8(c) presents the corresponding integrated PL intensity. From Fig. 8 it can be seen, that the PL intensity of the As-terminated GaAs with 10 nm Al_2O_3 layer (sample As-10-st) increases only by a factor of two compared to the non-passivated air-exposed GaAs substrate. The reason for this behaviour can be found by analyzing the As $2p_{3/2}$ photoelectron spectrum (Fig. 3(b)), which shows the presence of the As–As dimers at the Al_2O_3/GaAs interface. An earlier first-principles study of GaAs surfaces and

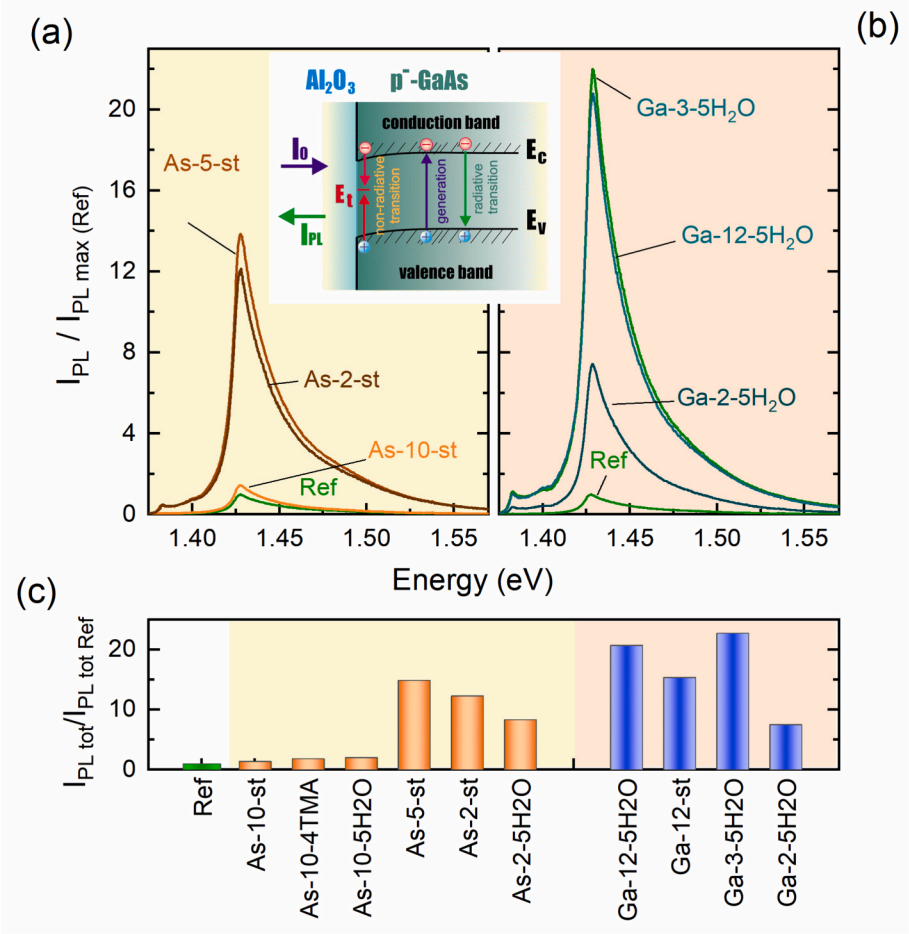

Fig. 8. PL intensity (a) and (b) integrated PL intensity (c) of the native oxides/GaAs (Ref) and Al_2O_3/GaAs samples. Inset: Illustration of the PL method for characterization of the Al_2O_3/GaAs interface states. Here E_c is the conduction band minimum, E_v is the valence band maximum, E_t is the interface defect state, I_0 is the excitation light intensity, and I_{PL} is the PL intensity.

interfaces [62] demonstrates that the transformation between an As–As dimer and two doubly occupied As dangling bonds is the dominant process responsible for charge trapping. In our particular case, this implies that the As–As dimers near the interface trap photogenerated charge carriers, leading to the low PL response of the As-10-st sample. The low-valence As oxides present at the interface do not contribute states to the band gap [9,48] and thus cannot affect the radiative recombination. In addition, we confirmed the inefficiency of the *in situ* passivation of the As-terminated GaAs substrate with an Al_2O_3 layer thicker than 10 nm by PL measurements of GaAs/AlGaAs multiple quantum well structures (Section 6 in the SI).

The As-terminated sample with a deposited 5 nm Al_2O_3 layer (As-5-st) demonstrates a much stronger PL signal. We suggest that oxygen, diffusing through the Al_2O_3 layer partially decomposes the As–As dimers, causing the stronger PL response of the sample. However, further decrease in Al_2O_3 thickness results in degradation of the PL response. Indeed, oxygen from the ambient air can more easily diffuse through the thinner Al_2O_3 layer to reach the Al_2O_3/GaAs interface and oxidize the GaAs substrate. Elemental As, generated by the oxidation of the GaAs surface injects into GaAs as interstitials and As_{Ga} antisites, and is predicted by first-principles calculations to create bandgap defect states [5,45]. The formed defects mediate the non-radiative recombination leading to the degraded PL performance. The integrated intensity of the Ga-terminated GaAs samples with Al_2O_3 layer thickness above 3 nm increases by a factor of 20 compared to the GaAs sample with native oxides. The substantially better PL performance of the passivated Ga-terminated samples is not surprising considering the previous XPS data (Fig. 4). As–As dimers and elemental As free Al_2O_3/GaAs interface of Ga-12-5H_2O and Ga-3-5H_2O samples implies low density of band gap states which in turn leads to the high PL intensity. The lower PL intensity of Ga-2-5H_2O sample compared to Ga-12-5H_2O and Ga-3-5H_2O is due to the formation of elemental As in the near interface region mediated by post-deposition oxidation.

We attribute the larger PL intensity of the As-2-st sample compared to the Ga-2-5H_2O sample to the lower elemental As fraction at the Al_2O_3/GaAs interface (Figs. 5 and 6). This is due to the larger Al_2O_3 layer thickness (Table 1) of the As-2-st sample, thus weaker post-deposition interface oxidation in this case.

4. Conclusions

In conclusion, we have investigated the chemical composition of the interface formed during *in situ* atomic layer deposition of Al_2O_3 on an atomically clean (0 0 1) GaAs surface. Our results extend previous studies on GaAs surface passivation [12–35,63,64] by elucidating how the passivation properties of Al_2O_3 [65–68] can be effectively realized through *in situ* deposition. We reveal that the Al_2O_3 layer with a thickness exceeding 3 nm grown on the As-terminated (2 × 4) GaAs surface buries As–As bonds related to the As–As dimers and As dangling bonds. The low-valence As oxides, As_2O and AsO, are also formed. Whether the deposition starts with a TMA or a water pulse does not qualitatively affect the chemical composition at the interface. It is important to note that the remaining As–As dimers contribute states within the band gap and this eliminates effective passivation. Indeed, the room temperature

PL measurements show that the PL intensity of these samples is only two times higher than the corresponding intensity of the non-passivated GaAs sample with native oxides. In contrast, the deposition of Al_2O_3 on the Ga-terminated GaAs surface leads to the formation of an almost defect-free Al_2O_3/GaAs interface with only very small traces of As–As bonds and low-valence As oxides. These samples irradiated with a laser show a PL intensity that is significantly (about 20 times) stronger than the PL of the air-exposed non-passivated sample. This underlines the importance of the presence of As–As dimers in the formation of deep defects states at the interface. The reduction of the deposited Al_2O_3 layer thickness below 3 nm leads to a post-deposition oxidation of the GaAs surface due to oxygen diffusion through the oxide layer. We propose that the diffusing oxygen decomposes the As–As dimers remaining on the As-terminated GaAs, as the As $2p_{3/2}$ spectrum does no longer demonstrate their presence, which is surprising positive effect of the post-oxidation. However, due to the oxidation, we detect the formation of elemental As, which in turn induces states into the GaAs band gap. Despite the presence of the Ga and As oxides, Ga_2O_3, As_2O, AsO, As_2O_3, and As_2O_5, and elemental arsenic at the interface the PL intensity of the As- and Ga-terminated post-oxidized samples is still significantly (x10) higher than the PL intensity of the non-passivated samples and is determined by the density of elemental As formed. Analysis of As $2p_{3/2}$ and Ga $2p_{3/2}$ spectra shows that after oxide deposition, the band bending in GaAs at the Al_2O_3/GaAs interface is reduced by 0.2-0.4 eV, indicating the reduction of the interface state density, i.e. the unpinned state of the Fermi level at the interface.

CRediT authorship contribution statement

Nataliya Demarina: Writing – original draft, Supervision, Project administration, Investigation, Formal analysis, Data curation. **Soraya Karimzadah:** Investigation, Formal analysis, Data curation. **Benjamin Bennemann:** Writing – review & editing, Methodology, Investigation, Formal analysis, Data curation. **Christoph Krause:** Investigation, Data curation. **Abdur Rehman Jalil:** Writing – review & editing, Investigation, Formal analysis. **Heinrich Hartmann:** Writing – review & editing, Investigation, Formal analysis, Data curation. **Beata Kardynał:** Writing – review & editing, Supervision, Project administration, Investigation, Data curation, Conceptualization. **Mihail Ion Lepsa:** Investigation. **Detlev Gruetzmacher:** Writing – review & editing, Supervision, Project administration, Conceptualization.

Declaration of competing interest

The authors declare that they have no known competing financial interests or personal relationships that could have appeared to influence the work reported in this paper.

Appendix A. Supplementary material

Supplementary data to this article can be found online at https://doi.org/10.1016/j.apsusc.2025.165114.

Data availability

Data will be made available on request.

References

[1] K.Y. Cheng, III–V compound semiconductors and devices: an introduction to fundamentals, Springer (2020), https://doi.org/10.1007/978-3-030-51903-2.

[2] P. Laukkanen, M.P.J. Punkkinen, M. Kuzmin, K. Kokko, J. Lång, R.M. Wallace, Passivation of III–V surfaces with crystalline oxidation, Appl. Phys. Rev. 8 (2021) 011309, https://doi.org/10.1063/1.5126629.

[3] H. Hasegawa, M. Akazawa, Interface models and processing technologies for surface passivation and interface control in III–V semiconductor nanoelectronics, Appl. Surf. Sci. 254 (2008) 8005–8014, https://doi.org/10.1016/j.apsusc.2008.03.051.

[4] L. Zhou, B. Bo, X. Yan, C. Wang, Y. Chi, X. Yang, Brief review of surface passivation on III–V semiconductor, Crystals 8 (2018) 226, https://doi.org/10.3390/cryst8050226.

[5] J. Robertson, Y. Guo, L. Lin, Defect state passivation at III–V oxide interfaces for complementary metal–oxide–semiconductor devices, J. Appl. Phys. 117 (2015) 112806, https://doi.org/10.1063/1.4913832.

[6] W. Wang, C.L. Hinkle, E.M. Vogel, K. Cho, R.M. Wallace, Is interfacial chemistry correlated to gap states for high-k/III–V interfaces? Microelectron. Eng. 88 (2011) 1061–1065, https://doi.org/10.1016/j.mee.2011.03.053.

[7] D. Colleoni, G. Miceli, A. Pasquarello, Fermi-level pinning through defects at GaAs/oxide interfaces: a density functional study, Phys. Rev. B 92 (2015) 125304, https://doi.org/10.1103/PhysRevB.92.125304.

[8] L. Lin, J. Robertson, Passivation of interfacial defects at III–V oxide interfaces, J. Vac. Sci. Technol. B 30 (2012) 04E101, https://doi.org/10.1116/1.4710513.

[9] M. Scarrozza, G. Pourtois, M. Houssa, M. Caymax, M. Meuris, M.M. Heyns, A. Stesmans, Adsorption of molecular oxygen on the reconstructed β2(2×4)-GaAs (0 0 1) surface: a first-principles study, Surf. Sci. 603 (2009) 203–208, https://doi.org/10.1016/j.susc.2008.11.002.

[10] J. Gao, G. He, S. Liang, D. Wang, B. Yang, Comparative study on in situ surface cleaning effect of intrinsic oxide-covering GaAs surface using TMA precursor and Al_2O_3 buffer layer for HfGdO gate dielectrics, J. Mater. Chem. C 6 (2018) 2546–2551, https://doi.org/10.1039/C8TC00070K.

[11] R.L. Puurunen, Surface chemistry of atomic layer deposition: a case study for the trimethylaluminum/water process, J. Appl. Phys. 97 (2005) 121301, https://doi.org/10.1063/1.1940727.

[12] C.L. Hinkle, A.M. Sonnet, E.M. Vogel, S. McDonnell, G.J. Hughes, M. Milojevic, B. Lee, F.S. Aguirre-Tostado, K.J. Choi, H.C. Kim, J. Kim, R.M. Wallace, GaAs interfacial self-cleaning by atomic layer deposition, Appl. Phys. Lett. 92 (2008) 071901, https://doi.org/10.1063/1.2883956.

[13] C.L. Hinkle, M. Milojevic, E.M. Vogel, R.M. Wallace, Surface passivation and implications on high mobility channel performance (invited paper), Microelectron. Eng. 86 (2009) 1544–1548, https://doi.org/10.1016/j.mee.2009.03.030.

[14] M. Milojevic, C.L. Hinkle, F.S. Aguirre-Tostado, H.C. Kim, E.M. Vogel, J. Kim, R. M. Wallace, Half-cycle atomic layer deposition reaction studies on passivated GaAs (100) surfaces, Appl. Phys. Lett. 93 (2008) 252905, https://doi.org/10.1063/1.3054348.

[15] C.L. Hinkle, A.M. Sonnet, M. Milojevic, F.S. Aguirre-Tostado, H.C. Kim, J. Kim, R. M. Wallace, E.M. Vogel, Comparison of n-type and p-type GaAs oxide growth and its effects on frequency dispersion characteristics, Appl. Phys. Lett. 93 (2008) 113506, https://doi.org/10.1063/1.2987428.

[16] C.L. Hinkle, M. Milojevic, B. Brennan, A.M. Sonnet, F.S. Aguirre-Tostado, G. J. Hughes, E.M. Vogel, R.M. Wallace, Detection of Ga suboxides and their impact on III–V passivation and fermi-level pinning, Appl. Phys. Lett. 94 (2009) 162101, https://doi.org/10.1063/1.3120546.

[17] M. Tallarida, C. Adelmann, A. Delabie, S. Van Elshocht, M. Caymax, D. Schmeisser, Surface chemistry and fermi level movement during the self-cleaning of GaAs by trimethyl-aluminum, Appl. Phys. Lett. 99 (2011) 042906, https://doi.org/10.1063/1.3615784.

[18] C.-C. Cheng, C.-H. Chien, G.-L. Luo, C.-H. Yang, C.-C. Chang, C.-Y. Chang, C.-C. Kei, C.-N. Hsiao, T.-P. Perng, Effects of Interfacial sulfidization and thermal annealing on the electrical properties of an atomic-layer-deposited gate dielectric on GaAs substrate, J. Appl. Phys. 103 (2008) 074102, https://doi.org/10.1063/1.2891700.

[19] C.-W. Cheng, J. Hennessy, D. Antoniadis, E.A. Fitzgerald, Self-cleaning and surface recovery with arsine pretreatment in ex situ atomic-layer-deposition of Al_2O_3 on GaAs, Appl. Phys. Lett. 95 (2009) 082106, https://doi.org/10.1063/1.3213545.

[20] H.D. Lee, T. Feng, L. Yu, D. Mastrogiovanni, A. Wan, T. Gustafsson, E. Garfunkel, Reduction of native oxides on GaAs during atomic layer growth of Al_2O_3, Appl. Phys. Lett. 94 (2009) 222108, https://doi.org/10.1063/1.3148723.

[21] A.J. Henegar, T. Gougousi, Comparison of the reactivity of alkyl and alkyl amine precursors with native oxide GaAs(100) and InAs(100) surfaces, Appl. Surf. Sci. 390 (2016) 870–881, https://doi.org/10.1016/j.apsusc.2016.08.144.

[22] R.E. Sah, C. Tegenkamp, M. Baeumler, F. Bernhardt, R. Driad, M. Mikulla, O. Ambacher, Characterization of Al_2O_3/GaAs Interfaces and thin films prepared by atomic layer deposition, J. Vac. Sci. Technol. B 31 (2013) 04D111, https://doi.org/10.1116/1.4813436.

[23] Y.-S. Kang, D.-K. Kim, K.-S. Jeong, M.-H. Cho, C.Y. Kim, K.-B. Chung, H. Kim, D.-C. Kim, Structural evolution and the control of defects in atomic layer deposited HfO_2–Al_2O_3 stacked films on GaAs, ACS Appl. Mater. Interfaces 5 (2013) 1982–1987, https://doi.org/10.1021/am302803f.

[24] A. Werbrouck, M. Shirazi, F. Mattelaer, S.D. Elliott, J. Dendooven, C. Detavernier, A secondary reaction pathway for the alumina atomic layer deposition process with trimethylaluminum and water, revealed by full-range, time-resolved in situ mass spectrometry, J. Phys. Chem. C 124 (2020) 26443–26454, https://doi.org/10.1021/acs.jpcc.0c07602.

[25] B.A. Sperling, B. Kalanyan, J.E. Maslar, Using trimethylaluminum and H_2O: the kinetics of the H_2O half-cycle, J. Phys. Chem. C 124 (2020) 3410–3420, https://doi.org/10.1021/acs.jpcc.9b11291.

[26] S. Klejna, S.D. Elliott, First-principles modeling of the “clean-up” of native oxides during atomic layer deposition onto III–V substrates, J. Phys. Chem. C 116 (2012) 643–654, https://doi.org/10.1021/jp206566y.

[27] S. Klejna, S.D. Elliott, Atomistic decomposition of metal alkylamides, alkyls, and halides at reducible oxide surfaces: mechanism of ‘clean-up’ during atomic layer deposition of dielectrics onto III–V substrates, Chem. Mater. 26 (2014) 2427–2437, https://doi.org/10.1021/cm403336c.

[28] T.W. Pi, H.Y. Lin, Y.T. Liu, T.-D. Lin, G. Wertheim, J. Kwo, M. Hong, Atom-to-atom interactions for atomic layer deposition of trimethylaluminum on Ga-rich GaAs(0

0 1)-4×6 and As-rich GaAs(0 0 1)-2×4 surfaces: a synchrotron radiation photoemission study, Nanoscale Res. Lett. 8 (2013) 169, https://doi.org/10.1186/1556-276X-8-169.
[29] Y.H. Chang, M.L. Huang, C.L. Hsu, T.W. Pi, M. Hong, J. Kwo, In situ atomic layer deposition and synchrotron radiation photoemission study of Al2O3 on pristine n-GaAs(0 0 1)-4×6 surface, Microelectron. Eng. 88 (2011) 1101–1104, https://doi.org/10.1016/j.mee.2011.03.064.
[30] M.L. Huang, Y.H. Chang, T.D. Lin, H.Y. Lin, Y.T. Liu, T.W. Pi, M. Hong, J. Kwo, Growth mechanism of atomic layer deposited Al_2O_3 on GaAs(0 0 1)-4×6 surface with trimethylaluminum and water as precursors, Appl. Phys. Lett. 101 (2012) 212101, https://doi.org/10.1063/1.4767129.
[31] T.W. Pi, W.S. Chen, Y.H. Lin, Y.T. Cheng, G.J. Wei, K.Y. Lin, C.-P. Cheng, J. Kwo, M. Hong, Surface atoms core-level shifts in single crystal gaas surfaces: interactions with trimethylaluminum and water prepared by atomic layer deposition, Appl. Surf. Sci. 284 (2013) 601–610, https://doi.org/10.1016/j.apsusc.2013.07.140.
[32] T.W. Pi, Y.H. Lin, Y.T. Fanchiang, T.H. Chiang, C.H. Wei, Y.C. Lin, G.K. Wertheim, J. Kwo, M. Hong, In-situ atomic layer deposition of trimethylaluminum and water on pristine single-crystal (In)GaAs surfaces: electronic and electric structures, Nanotechnology 26 (2015) 164001, https://doi.org/10.1088/0957-4484/26/16/164001.
[33] Y.-T. Fanchiang, T.-H. Chiang, T.-W. Pi, G.K. Wertheim, J.R. Kwo, M. Hong, Reconstruction at the interface of one cycle of trimethylaluminum and water on GaAs(111)A-2×2 from atomic layer deposition, Appl. Phys Express 8 (2015) 126602, https://doi.org/10.7567/APEX.8.126602.
[34] T.W. Chang, K.Y. Lin, Y.H. Lin, L.B. Young, J. Kwo, M. Hong, Analysis of border and interfacial traps in ALD-Y2O3 and -Al2O3 on GaAs via electrical responses – a comparative study, Microelectron. Eng. 178 (2017) 199–203, https://doi.org/10.1016/j.mee.2017.05.019.
[35] T.W. Pi, W.S. Chen, Y.H. Lin, Y.T. Cheng, G.J. Wei, K.Y. Lin, C.-P. Cheng, J. Kwo, M. Hong, Relevance of GaAs(0 0 1) surface electronic structure for high frequency dispersion on N-type accumulation capacitance, Appl. Phys. Lett. 110 (2017) 052107, https://doi.org/10.1063/1.4975479.
[36] A. Ohtake, Surface reconstructions on GaAs(0 0 1), Surf. Sci. Rep. 63 (2008) 295–327, https://doi.org/10.1016/j.surfrep.2008.03.001.
[37] S. Tanuma, C.J. Powell, D.R. Penn, Calculations of electron inelastic mean free paths, Surf. Interface Anal. 17 (1991) 927–939, https://doi.org/10.1002/sia.1997.
[38] C.L. Hinkle, M. Milojevic, E.M. Vogel, R.M. Wallace, The significance of core-level electron binding energies on the proper analysis of InGaAs interfacial bonding, Appl. Phys. Lett. 95 (2009) 151905, https://doi.org/10.1063/1.3249577.
[39] M.P.J. Punkkinen, P. Laukkanen, K. Kokko, M. Ropo, M. Ahola-Tuomi, I. J. Vayrynen, H.-P. Komsa, T.T. Rantala, M. Pessa, M. Kuzmin, L. Vitos, J. Kollar, B. Johansson, Surface core-level shifts of GaAs (100) (2×4) from first principles, Phys. Rev. B 76 (2007) 115334, https://doi.org/10.1103/PhysRevB.76.115334.
[40] M. Scarrozza, G. Pourtois, M. Houssa, M. Caymax, A. Stesmans, M. Meuris, M. M. Heyns, A theoretical study of the initial oxidation of the GaAs(0 0 1) – β2(2×4) surface, Appl. Phys. Lett. 95 (2009) 253504, https://doi.org/10.1063/1.3275737.
[41] S. McDonnell, H. Dong, J.M. Hawkins, B. Brennan, M. Milojevic, F.S. Aguirre-Tostado, D.M. Zhernokletov, C.L. Hinkle, J. Kim, R.M. Wallace, interfacial oxide re-growth in thin film metal oxide III-V semiconductor systems, Appl. Phys. Lett. 100 (2012) 141606, https://doi.org/10.1063/1.3700863.
[42] A. Stesmans, S. Nguyen, V. V. Afanas'ev, As_{Ga}+ Antisites Identified by Electron Spin Resonance as a Main Interface Defect System in Thermal GaAs/Native Oxide Structures, Appl. Phys. Lett. 103 (2013) 162111. doi: 10.1063/1.4824881.
[43] G.P. Schwartz, Analysis of native oxide films and oxide-substrate reactions on III–V semiconductors using thermochemical phase diagrams, Thin Solid Films 103 (1983) 3–16, https://doi.org/10.1016/0040-6090(83)90420-0.
[44] J.E. Northrup, S. Froyen, Surface structure of GaAs(0 0 1) surfaces: the role of electrostatic interactions, Phys. Rev. B 50 (1994) 2015–2020, https://doi.org/10.1103/PhysRevB.50.2015.
[45] G. Miceli, A. Pasquarello, First principles study of As 2p core-level shifts at GaAs/Al_2O_3 interfaces, Appl. Phys. Lett. 102 (2013) 201607, https://doi.org/10.1063/1.4807730).
[46] B. Brennan, G. Hughes, Interface Chemistry of ALD Identification and thermal stability of the native oxides on InGaAs using Synchrotron radiation based photoemission, J. Appl. Phys. 108 (2010) 053516, https://doi.org/10.1063/1.3475499.
[47] B. Brennan, M. Milojevic, C. L. Hinkle, F. S. Aguirre-Tostado, G. Hughes, R. M. Wallace, Optimisation of the Ammonium Sulphide (NH4)2S Passivation Process on In0.53Ga0.47As, Appl. Surf. Sci. 257 (2011) 4082–4089. doi: 10.1016/j.apsusc.2010.11.179.
[48] L. Lin, J. Robertson, Defect states at III-V semiconductor oxide interfaces, Appl. Phys. Lett. 98 (2011) 082903, https://doi.org/10.1063/1.3556619.
[49] Y.C. Chang, C. Merckling, J. Penaud, C.Y. Lu, W.-E. Wang, J. Dekoster, M. Meuris, M. Caymax, M. Heyns, J. Kwo, M. Hong, Effective reduction of interfacial traps in (0 0 1) gate stacks using surface engineering and thermal annealing, Appl. Phys. Lett. 97 (2010) 112901, https://doi.org/10.1063/1.3488813.
[50] Y.C. Chang, W.H. Chang, C. Merckling, J. Kwo, M. Hong, Inversion-channel GaAs (100) MOSFETs using ALD-Deposited Al_2O_3 as gate dielectrics, Appl. Phys. Lett. 102 (2013) 093506, https://doi.org/10.1063/1.4793433.
[51] M.D. Pashley, Electron counting model and its application to island structures on molecular-beam epitaxy grown GaAs(0 0 1) and ZnSe(0 0 1), Phys. Rev. B 40 (1989) 10481–10487, https://doi.org/10.1103/PhysRevB.40.10481.
[52] X. Zhang, S. Ptasinska, Dissociative Adsorption of Water on an H_2O/GaAs(100) Interface: In Situ Near-Ambient Pressure XPS Studies, J. Phys. Chem. C 118 (2014) 4259–4266. doi: 10.1021/jp411977p.
[53] R. Nakamura, T. Toda, S. Tsukui, M. Tane, M. Ishimaru, T. Suzuki, H. Nakajima, Diffusion of oxygen in amorphous Al_2O_3, Ta_2O_5, and Nb_2O_5, J. Appl. Phys. 116 (2014) 033504, https://doi.org/10.1063/1.4889800.
[54] T. Nabatame, T. Yasuda, M. Nishizawa, M. Ikeda, T. Horikawa, A. Toriumi, Comparative studies on oxygen diffusion coefficients for amorphous and γ-Al_2O_3 films using ^{18}O isotope, Jpn. J. Appl. Phys. 42 (2003) 7205–7210, https://doi.org/10.1143/JJAP.42.7205.
[55] W.E. Spicer, I. Lindau, P. Skeath, C.Y. Su, Unified mechanism for Schottky-Barrier formation and III-V oxide interface states, Phys. Rev. Lett. 44 (1980) 420–423, https://doi.org/10.1103/PhysRevLett.44.420.
[56] W.E. Spicer, I. Lindau, P. Skeath, C.Y. Su, Unified defect model and beyond, J. Vac. Sci. Technol. 17 (1980) 1019–1027, https://doi.org/10.1116/1.570583.
[57] H. Yamaguchi, Y. Horikoshi, Surface-defect formation on heavily doped InAs and GaAs layers studied by scanning tunneling microscopy, Phys. Rev. B 53 (1996) 4565–4574, https://doi.org/10.1103/PhysRevB.53.4565.
[58] P.A. Alekseev, M.S. Dunaevskiy, G.E. Cirlin, R.R. Reznik, A.N. Smirnov, D. A. Kirilenko, V.Y. Davydov, V.L. Berkovits, Unified mechanism of the surface fermi level pinning in III-As nanowires, Nanotechnology 29 (2018) 314003, https://doi.org/10.1088/1361-6528/aac480.
[59] T. Saitoh, H. Iwadate, H. Hasegawa, In situ surface state spectroscopy by photoluminescence and surface current transport for compound semiconductors, Jpn. J. Appl. Phys. 30 (1991) 3750–3755, https://doi.org/10.1143/JJAP.30.3750.
[60] M. Akazawa, A. Domanowska, B. Adamowicz, H. Hasegawa, Capacitance-voltage and photoluminescence study of high-k/GaAs interfaces controlled by Si interface control layer, J. Vac. Sci. Technol. B 27 (2009) 2028–2035, https://doi.org/10.1116/1.3167361.
[61] I.H. Campbell, P.M. Fauchet, CW laser irradiation of GaAs: arsenic formation and photoluminescence degradation, Appl. Phys. Lett. 57 (1990) 10–12, https://doi.org/10.1063/1.103564.
[62] D. Colleoni, G. Miceli, A. Pasquarello, Origin of fermi-level pinning at GaAs surfaces and interfaces, J. Phys. Condens. Matter 26 (2014) 492202, https://doi.org/10.1088/0953-8984/26/49/492202.
[63] Q. Lin, J. Huang, Y. Xue, L. Lin, Z. Xing, K.S. Wong, K.M. Lau, GaAs microdisk lasers with Al_2O_3 passivation selectively grown on SOI, ACS Photonics 11 (2024) 3578, https://doi.org/10.1021/acsphotonics.4c00527.
[64] R.J. Theeuwes, W.M.M. Kessels, B. Macco, Surface passivation approaches for silicon, germanium, and III–V semiconductors, J. Vac. Sci. Technol. A 42 (2024) 060801, https://doi.org/10.1116/6.0004030.
[65] D. Colleoni, G. Miceli, A. Pasquarello, Band alignment and chemical bonding at the GaAs/Al_2O_3 interface: a hybrid functional study, Appl. Phys. Lett. 107 (2015) 211601, https://doi.org/10.1063/1.4936240.
[66] N.V. Nguyen, O.A. Kirillov, W. Jiang, W. Wang, J.S. Suehle, P.D. Ye, Y. Xuan, N. Goel, K.-W. Choi, W. Tsai, S. Sayan, Band offsets of atomic-layer-deposited on gaas and the effects of surface treatment, Appl. Phys. Lett. 93 (2008) 082105, https://doi.org/10.1063/1.2976676.
[67] M. Choi, A. Janotti, C.G. Van de Walle, Native point defects and dangling bonds in α-Al_2O_3, J. Appl. Phys. 113 (2013) 044501, https://doi.org/10.1063/1.4784114.
[68] B. Nalcaci, P.M. Gonullu, Insight of mechanical and morphological properties of ALD- Al_2O_3 films in point of structural properties, Appl. Phys. A 127 (2021) 460, https://doi.org/10.1007/s00339-021-04601-x.